Severe hepatocellular disease in mice lacking one or both *CaaX* prenyltransferases[S]

Shao H. Yang,* Sandy Y. Chang,* Yiping Tu,* Gregory W. Lawson,[§] Martin O. Bergo, Loren G. Fong,[1,*] and Stephen G. Young[1,*,†]**

Departments of Medicine* and Human Genetics,[†] Division of Laboratory Animal Medicine,[§] University of California, Los Angeles, CA 90095; and Sahlgrenska Cancer Center,** Institute of Medicine, University of Gothenburg, Gothenburg, Sweden

Abstract Protein farnesyltransferase (FTase) and protein geranylgeranyltransferase-I (GGTase-I) add 15- or 20-carbon lipids, respectively, to proteins that terminate with a *CaaX* motif. These posttranslational modifications of proteins with lipids promote protein interactions with membrane surfaces in cells, but the in vivo importance of the *CaaX* prenyltransferases and the protein lipidation reactions they catalyze remain incompletely defined. One study concluded that a deficiency of FTase was inconsequential in adult mice and led to little or no tissue pathology. To assess the physiologic importance of the *CaaX* prenyltransferases, we used conditional knockout alleles and an albumin–*Cre* transgene to produce mice lacking FTase, GGTase-I, or both enzymes in hepatocytes. The hepatocyte-specific FTase knockout mice survived but exhibited hepatocellular disease and elevated transaminases. Mice lacking GGTase-I not only had elevated transaminases but also had dilated bile cannaliculi, hyperbilirubinemia, hepatosplenomegaly, and reduced survival. Of note, GGTase-I–deficient hepatocytes had a rounded shape and markedly reduced numbers of actin stress fibers. Hepatocyte-specific FTase/GGTase-I double-knockout mice closely resembled mice lacking GGTase-I alone, but the disease was slightly more severe.[JLR] Our studies refute the notion that FTase is dispensable and demonstrate that GGTase-I is crucial for the vitality of hepatocytes.—Yang, S. H., S. Y. Chang, Y. Tu, G. W. Lawson, M. O. Bergo, L. G. Fong, and S. G. Young. **Severe hepatocellular disease in mice lacking one or both *CaaX* prenyltransferases. *J. Lipid Res.* 2012.** 53: **77–86.**

Supplementary key words protein farnesyltransferase • protein geranylgeranyltransferase • hyperbilirubinemia • hepatic steatosis • prelamin A • actin stress fibers

Protein farnesyltransferase (FTase) and protein geranylgeranyltransferase-I (GGTase-I) add 15-carbon farnesyl or 20-carbon geranylgeranyl lipids, respectively, to the cysteine in proteins that terminate with a *CaaX* motif ("*C*" is a cysteine; "*a*" is often an aliphatic amino acid; the "*X*" can be one of many residues). This posttranslational modification is generally called "protein prenylation" (1, 2). Cell culture studies have demonstrated that protein prenylation promotes the ability of proteins to associate with membrane surfaces (2). For example, when the farnesylation of H-RAS (a proto-oncogene implicated in the pathogenesis of human cancers) is eliminated, the protein loses its ability to reach the plasma membrane and relay the signals that promote cell growth (3–5). These studies prompted the pharmaceutical industry to develop FTase inhibitors (FTIs) for the treatment of cancer (6–9). GGTase-I inhibitors (GGTIs) and dual FTase/GGTase-I inhibitors have also been developed as potential anticancer therapies (10, 11).

Despite considerable interest in FTase as a therapeutic target, the in vivo importance of FTase for the vitality of mammalian cells and tissues has never been clearly defined. One group developed a knockout allele for *Fntb* (encoding the β-subunit of FTase) and concluded that FTase is required for embryonic development but that FTase deficiency is associated with little or no pathology in adult tissues (12). The authors suggested that the dispensability of FTase in the tissues of adult mice might relate, in part, to alternate prenylation of FTase substrates by

This work was supported by National Institutes of Health Grants HL-76839, CA-099506-07, HL-086683, and HL-089781; Ellison Medical Foundation Senior Scholar Program; March of Dimes Grant 6-FY2007-1012; American Heart Association, Western States Affiliate, Beginning Grant-in-Aid 0865262F; and Vascular Biology Program, UCLA, Fellowship 2 T32 HL069766:06. Its contents are solely the responsibility of the authors and do not necessarily represent the official views of the National Institutes of Health.

Manuscript received 3 October 2011.

Published, JLR Papers in Press, October 28, 2011
DOI 10.1194/jlr.M021220

Abbreviations: ALP, alkaline phosphatase; ALT, alanine aminotransferase; AST, aspartate aminotransferase; *Fntb*, mouse gene for the β-subunit of protein farnesyltransferase; FTase, protein farnesyltransferase; FTI, protein farnesyltransferase inhibitor; GGTase-I, protein geranylgeranyltransferase-I; GGTI, protein geranylgeranyltransferase inhibitor; *Pggt1b*, mouse gene for the β-subunit of protein geranylgeranyltransferase-I.

[1] To whom correspondence should be addressed.
e-mail: sgyoung@mednet.ucla.edu (S.G.Y.); lfong@mednet.ucla.edu (L.G.F.)

[S] The online version of this article (available at http://www.jlr.org) contains supplementary data in the form of seven figures.

GGTase-I (12). The conclusion that FTase is dispensable in adult tissues was somewhat surprising, considering the importance of this enzyme in yeast (13, 14). Nevertheless, the notion that FTase was not essential for mammalian cells and tissues seemed consistent with preclinical studies of FTIs, which were reported to have few adverse side effects (15, 16). But newer studies raised uncertainties about the notion that FTase is dispensable. A deficiency of FTase in keratinocytes led to severe alopecia (17). The fact that FTase deficiency caused significant pathology in one study (17) but not in another (12) indicated a need for additional studies on the physiologic importance of FTase in mammalian tissues.

The physiologic consequences of GGTase-I deficiency are also poorly defined. Early studies with GGTIs indicated that they were quite toxic (11). That finding, together with the observation that GGTase-I deficiency is lethal in budding yeast (13), led many to suspect that GGTase-I would be an essential protein in mammalian cells. However, more recent studies of GGTase-I inhibitors have found less toxicity (18, 19), and genetic models of GGTase-I deficiency (with a conditional knockout allele for *Pggt1b*, which encodes the β-subunit of GGTase-I) suggested that mammalian cells can survive in the absence of GGTase-I (20, 21). For example, inactivating GGTase-I in mouse pneumocytes retarded the growth of lung tumors without toxicity to normal lung tissue (20). Although GGTase-I–deficient lung tumors grew at a slower rate, they ultimately became quite large and caused the mice to die, implying that GGTase-I–deficient cells can survive in vivo (20). More recently, Khan et al. (22) created mice lacking GGTase-I in macrophages and found that GGTase-I–deficient macrophages were activated, leading to erosive arthritis. These genetic studies, along with conflicting information on the properties of GGTIs, underscored a need for a fresh look at the functional relevance of GGTase-I in mammalian cells.

Given the uncertainties about the functional importance of both FTase and GGTase-I in mammals, we decided to assess the impact of deficiencies of the two protein prenyltransferases, alone and in combination, in hepatocytes. We chose hepatocytes for three reasons. The first is that one can obtain very efficient recombination—and efficient gene inactivation—with the albumin–*Cre* transgene (23, 24). The second is that abnormalities in hepatocyte function can be readily detected with simple blood tests and histological studies. Third, it is straightforward to isolate and analyze hepatocytes from mouse models.

MATERIALS AND METHODS

Hepatocyte-specific *Fntb* and *Pggt1b* knockout mice

A conditional knockout allele for *Fntb*, $Fntb^{fl}$, was recently generated by Liu et al. (21). *Cre*-mediated excision of the "floxed" segment of DNA removes the *Fntb* promoter, the translational start site, and exon 1. $Fntb^{+}$ and $Fntb^{fl}$ alleles were identified by PCR with forward primer 5′–AGGATTTGGGTGAGGGAA–3′ and reverse primer 5′–AGCAGCCACCTGGAGACT–3′; $Fntb^{+}$ and $Fntb^{fl}$ alleles yielded 250- and 320-bp amplicons, respectively. Mice harboring a *Pggt1b* conditional knockout allele, $Pggt1b^{fl}$ (20), were also used. Both $Fntb^{fl/fl}$ and $Pggt1b^{fl/fl}$ mice were bred with albumin–Cre (*AlbCre*) transgenic mice (24). In this article, hepatocyte-specific *Fntb* knockout mice ($Fntb^{fl/fl}$*AlbCre*) were designated "$Fntb^{\Delta/\Delta}$ mice"; hepatocyte-specific *Pggt1b* knockout mice ($Pggt1b^{fl/fl}$*AlbCre*) were designated "$Pggt1b^{\Delta/\Delta}$ mice." The *AlbCre* transgene was detected by PCR with forward primer 5′–GCATTACCGGTCGATGCAACGAGTGATGAG–3′ and reverse primer 5′–GAGTGAACGAACCTGGTCGAAATCAGTGCG–3′.

Mice were weaned at 21 days of age, housed in a virus-free barrier facility with a 12-h light-dark cycle, and fed a chow diet containing 4.5% fat. All experiments were approved by UCLA's Animal Research Committee.

Mouse primary hepatocytes

Primary hepatocytes were isolated by a two-step perfusion protocol based on previously described methods (25, 26). Briefly, mice were anesthetized by intraperitoneal injection of pentobarbitone (50 mg/kg). The abdominal cavity was opened and the liver was perfused via the portal vein, first with 37°C 10 mM HEPES-buffered saline for 5 min, and subsequently with 37°C 0.05% type I collagenase (Worthington Biochemical Corp., Lakewood, NJ) in 10 mM HEPES-buffered saline for 7 min at 5 ml/min. After perfusion, the liver was excised and chopped with scissors in Hepato-STIM medium (BD Biosciences, San Jose, CA) to disperse the cells. A series of five low-speed (50 *g*) centrifugation steps was performed to enrich the population of hepatocytes (and limit numbers of Kupffer and endothelial cells). The resulting cell pellet was resuspended, and an aliquot was taken to assess cell number and viability (by trypan blue exclusion). Hepatocyte preparations were then plated at a density of 2.0×10^6 cells on 60-mm collagen-coated plates (BD Biosciences) in Hepato-STIM medium containing 10% FBS (ATCC, Manassas, VA) containing pen/strep (ATCC) and Fungizone (Invitrogen, Carlsbad, CA) and allowed to adhere for 4 h. The medium was then removed; the cells washed with PBS and fresh medium was added.

Extraction of RNA, cDNA synthesis, and RT-PCR

Total RNA was extracted from freshly prepared primary hepatocytes with TRI reagent (Molecular Research Center), treated with DNase I (Ambion, Applied Biosystems), and reverse-transcribed with SuperScript III (Invitrogen). qRT-PCR reactions were performed on a 7900HT Fast Real-Time PCR System (Applied Biosystems) with 50 ng cDNA, 200 nM oligonucleotides, and 10 μl SensiMixPlus SYBR (Bioline). Expression levels were calculated with the comparative cycle threshold method (27) and normalized to β2-microglobulin. To assess *Fntb* expression, we used oligonucleotide primers 5′–GACGGCTGCTACTCCTTCTG–3′ and 5′–TGCTGATGGAACATCCAATG–3′; for *Pggt1b* expression, we used primers 5′–GGGCATGGATATGAAGAAAGC–3′ and 5′–AAGGTGGATCCTCCATGAGAC–3′; for β2-microglobulin, we used primers 5′–TGGTGCTTGTCTCACTGACC–3′ and 5′–TATGTTCGGCTTCCCATTCT–3′.

Histology and immunohistochemistry

Livers were fixed in 10% paraformaldehyde (PFA), dehydrated for 24 h in 70% ethanol, and embedded in paraffin. Hematoxylin and eosin, Masson's trichrome, Sirius red, Periodic acid-Schiff (PAS), and reticulin stains were performed by UCLA's Department of Pathology. Oil Red O staining for neutral lipids was performed on frozen sections. For immunofluorescence studies, livers were embedded in Sakura Tissue-Tec OCT compound, frozen on dry ice, and 8-μm thick sections were cut with a cryostat. Sections were fixed in 3% PFA for 10 min, permeabilized with PBS containing 0.1% Tween-20, and incubated in blocking

buffer (PBS containing 10% fetal bovine serum, 0.2% BSA, 1 mM $CaCl_2$, and 1 mM $MgCl_2$) for 1 h. Sections were then incubated for 1 h at 4°C with Alexa Fluor 488–labeled phalloidin (1:200, Invitrogen) diluted in blocking buffer containing 0.2% Triton X-100. After washing the slides, the tissue sections were postfixed with 3% PFA for 10 min, incubated in PBS/DAPI for 10 min, washed twice with PBS, and then mounted with Prolong-Gold Antifade reagent (Invitrogen).

For immunocytochemical studies on primary hepatocytes, cells were grown on collagen I–coated cover slips (BD Biosciences), fixed in 3% PFA, permeabilized with 0.2% Triton X-100, and blocked with PBS containing 10% fetal bovine serum and 0.2% BSA (28). Cells were incubated for 2 h with primary antibodies. After washing, cells were incubated with secondary antibodies for 1 h. After washing, slides were mounted with ProLong Gold antifade reagent with DAPI (Invitrogen). The following antibodies and probes were used: lamin A (rabbit, 1:200, Santa Cruz Biotechnology); prelamin A (7G11, 1:50) (29); Alexa Fluor α-tubulin (1:400, Invitrogen); and Alexa Fluor 488–phalloidin (1:200, Invitrogen). Alexa Fluor 488– and Alexa Fluor 568–conjugated secondary antibodies were used at a 1:200 dilution.

Images were recorded with an Axiovert 200M microscope equipped with an AxioCam MRm and an ApoTome (all from Zeiss). Nuclear shape (2,000 cells/genotype) was assessed in a blinded fashion as described (29–32).

Protein extraction and Western blots

Protein extracts were prepared from primary hepatocytes with a urea-containing solubilization buffer (28, 33). Proteins were size-fractionated on 4–12% polyacrylamide Bis-Tris gels (Invitrogen) and then transferred to nitrocellulose for Western blotting. We used antibodies for the following proteins: lamin A/C (goat, 1:400, Santa Cruz Biotechnology); FTaseβ (rabbit, 1:200, Santa Cruz Biotechnology); HDJ-2 (mouse, 1:400, NeoMarkers); actin (goat, 1:1000, Santa Cruz Biotechnology); RAP1A (goat, 1:200, Santa Cruz Biotechnology); and prelamin A (29). After washing, the membranes were incubated with 1:5000 IRDye secondary antibodies (Rockland). Signals were detected with an Odyssey infrared imaging scanner (Li-Cor Biosciences).

Flow cytometry and cell sorting

Freshly prepared primary hepatocytes were analyzed by flow cytometry in UCLA's Flow Cytometry Laboratory (http://cyto.mednet.ucla.edu/). Briefly, cells were stained with propidium iodide (PI) and analyzed on a FACScan flow cytometer (BD Biosciences). Cell cycle analysis was performed with ModFit LT software (Verity Software House, Topsham, ME). To segregate cells based on DNA content, samples were sorted on a BD FACSAriaII sorter (BD Biosciences), and PI fluorescence was collected after a 670 LP filter with a 695/40-nm BP filter.

In vivo detection of apoptosis

Active caspases 3 and 7 in hepatocytes were detected with an in vivo technique (FLIVO, Immunochemistry Technologies). FLIVO is a fluorescently labeled inhibitor of caspases 3 and 7 that binds to active caspases. Mice were injected via the tail vein with the fluorescent probe (FAM-FLIVO), and livers were excised and frozen 1 h later. Then 8-μm sections were cut and fixed for 10 min in 3% PFA. The slides were incubated in PBS/DAPI for 10 min, washed twice with PBS, and mounted with Prolong-Gold

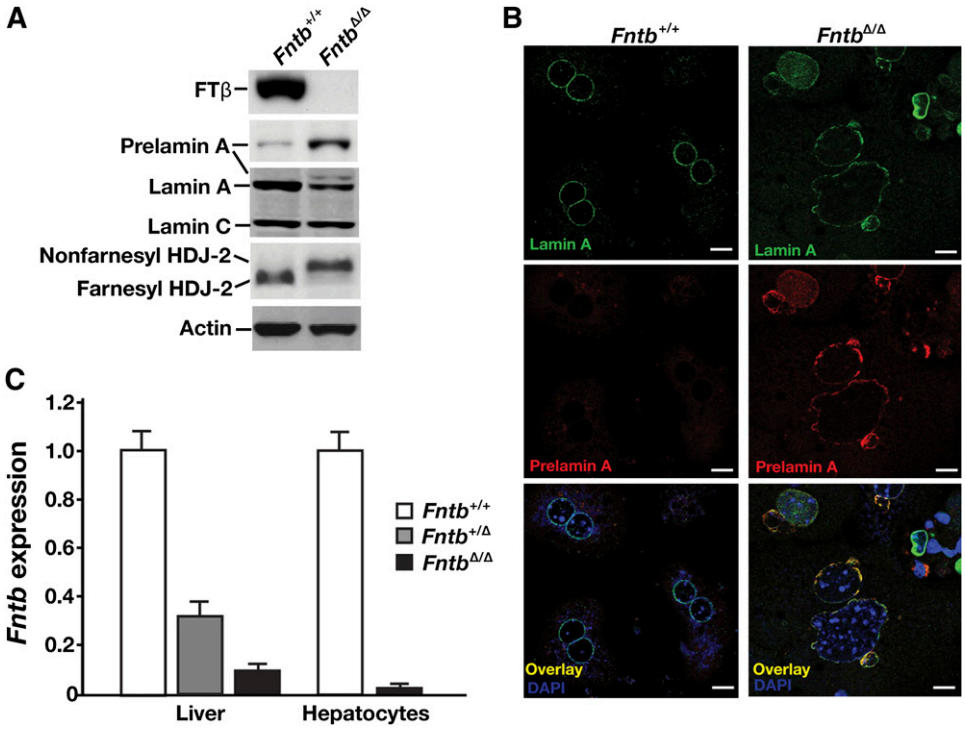

Fig. 1. Inactivating FTase in the liver. (A) Western blot of extracts from primary hepatocytes from *Fntb*$^{+/+}$ and *Fntb*$^{fl/fl}$*AlbCre*$^{+}$ (*Fntb*$^{\Delta/\Delta}$) mice with antibodies against the β-subunit of FTase (FTβ), prelamin A, lamin A/C, and HDJ-2. Actin was used as a loading control. (B) Immunohistochemical staining of primary hepatocytes from *Fntb*$^{+/+}$ and *Fntb*$^{\Delta/\Delta}$ mice with antibodies against lamin A (green) and prelamin A (red). DNA was visualized with DAPI (blue). Scale bar, 20 μm. (C) Quantitative RT-PCR analysis of *Fntb* expression with RNA prepared from whole liver or primary hepatocytes from *Fntb*$^{+/+}$, *Fntb*$^{fl/+}$*AlbCre*$^{+}$ (*Fntb*$^{+/\Delta}$), and *Fntb*$^{\Delta/\Delta}$ mice ($n = 4$ mice/group). Data were normalized to β2-microglobulin, and expression levels were compared with those of *Fntb*$^{+/+}$ mice (set at 1.0). Error bars indicate SEM.

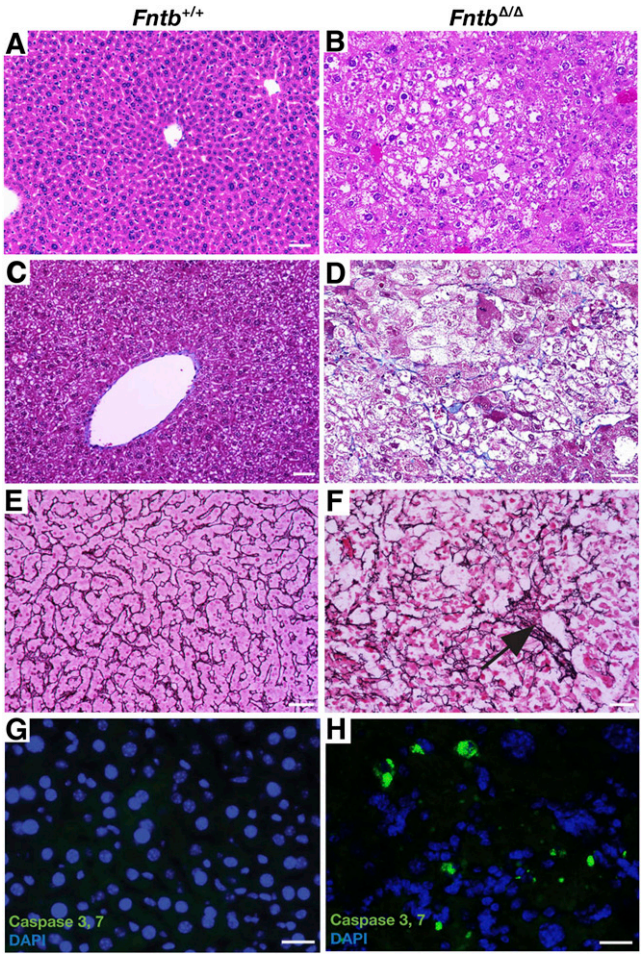

Fig. 2. *Fntb* deficiency in the liver causes steatosis, fibrosis, and apoptosis. (A, B) Hematoxylin and eosin–stained sections of liver from 12-month-old $Fntb^{+/+}$ and $Fntb^{\Delta/\Delta}$ mice, revealing disordered hepatic lobules and steatosis in $Fntb^{\Delta/\Delta}$ mice. (C, D) Masson's trichrome stain revealing increased collagen (blue) in the liver of the $Fntb^{\Delta/\Delta}$ mouse, along with steatosis and ballooning of hepatocytes. (E, F) Reticulin stain (black) revealing a disorganized liver architecture and regions with collapse of reticulin fibers (black arrow), corresponding to areas of hepatocyte loss. Images in A–F were recorded with a 20× objective. Scale bar, 50 μm. (G, H) Fluorescence microscopy revealing active caspases 3 and 7 in the livers of 6-month-old $Fntb^{+/+}$ and $Fntb^{\Delta/\Delta}$ mice (n = 3 mice/group were examined). Scale bar, 10 μm.

Antifade reagent (Invitrogen). The fluorescent signal (green) was imaged with an Axiovert 200M microscope equipped with an AxioCam MRm (Zeiss).

Liver cholesterol and triglyceride measurements

Neutral lipids were extracted from livers of $Fntb^{+/+}$ and $Fntb^{\Delta/\Delta}$ mice as described (34). Livers were weighed and homogenized in a 2:1 solution of chloroform and methanol. After 2-h incubation, 0.5 ml of 0.1 M NaCl was added, and the samples were mixed. After centrifugation, the organic phase was collected and dried. Samples were solubilized in ethanol containing 1% NP-40, and triglyceride and cholesterol levels were measured with enzymatic kits (Sigma Triglyceride kit and the Wako Cholesterol kit).

Statistical analyses

Body weight curves were compared with repeated-measures ANOVA and the log-rank test. Differences in the percentages of misshapen nuclei were assessed with a χ^2 test. Survival differences were assessed with a Kaplan-Meier test.

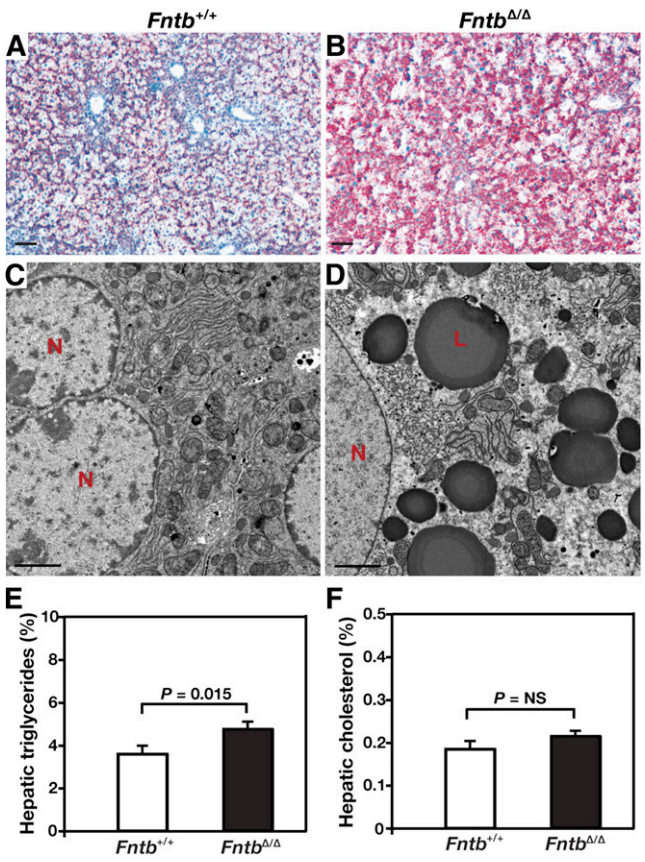

Fig. 3. Increased lipids in the liver of $Fntb^{\Delta/\Delta}$ mice. (A, B) Oil Red O–stained liver sections of 6-month-old $Fntb^{+/+}$ and $Fntb^{\Delta/\Delta}$ mice (n = 3 mice/group were examined). Sections were counterstained with Mayer's hematoxylin (blue). Scale bar, 100 μm. (C, D) Electron micrographs of livers from $Fntb^{+/+}$ and $Fntb^{\Delta/\Delta}$ mice. L, lipid droplets; N, nucleus. Magnification, ×14,000; scale bar, 2.0 μm. (E, F) Percentage triglycerides (E) and cholesterol (F) mass in livers of $Fntb^{+/+}$ and $Fntb^{\Delta/\Delta}$ mice (n = 8 mice/group). Error bars indicate SEM.

RESULTS

Hepatocyte-specific *Fntb* knockout mice

We used an *Fntb* conditional knockout allele, $Fntb^{fl}$, and an albumin–*Cre* (*AlbCre*) transgene to produce mice lacking *Fntb* in hepatocytes ($Fntb^{fl/fl}AlbCre^{+}$, designated $Fntb^{\Delta/\Delta}$ mice). *Cre*-mediated recombination was efficient; the β-subunit of FTase (FTβ) was undetectable in hepatocytes of $Fntb^{\Delta/\Delta}$ mice, as judged by Western blots with an FTβ-specific antibody (**Fig. 1A**). Also, protein farnesylation in hepatocytes was strongly inhibited, as judged both by an accumulation of nonfarnesylated HDJ-2 (Fig. 1A) and the appearance of prelamin A in cells (Fig. 1A, B). Consistent with these findings, *Fntb* transcript levels in $Fntb^{\Delta/\Delta}$ livers and isolated hepatocytes were very low (Fig. 1C).

$Fntb^{\Delta/\Delta}$ mice were born at the expected Mendelian frequency, appeared normal at birth, were fertile, and remained alive after 1 year of observation. However, $Fntb^{\Delta/\Delta}$

TABLE 1. Serum chemistry studies in wild-type and $Fntb^{\Delta/\Delta}$ mice

	Male			Female			
	Wild-type	$Fntb^{\Delta/\Delta}$	P	Wild-type	$Fntb^{\Delta/\Delta}$	P	Normal Range
ALT (U/L)	39 ± 5	531 ± 79	<0.0001	45 ± 6	462 ± 64	<0.0001	7–227
AST (U/L)	159 ± 36	585 ± 60	<0.0001	104 ± 20	546 ± 84	<0.0001	37–329
ALP (U/L)	37 ± 14	152 ± 17	<0.0001	68 ± 13	185 ± 28	<0.0001	13–291
CHOL (mg/dl)	80 ± 16	92 ± 24	NS	94 ± 8	102 ± 10	NS	34–219
GLU (mg/dl)	296 ± 27	183 ± 27	NS	232 ± 13	190 ± 14	NS	46–279
TRIG (mg/dl)	99 ± 10	89 ± 13	NS	153 ± 18	83 ± 7	NS	16–193
DBILI (mg/dl)	0.3 ± 0.01	0.2 ± 0.03	NS	0.3 ± 0.01	0.3 ± 0.01	NS	0–0.3
TBILI (mg/dl)	0.4 ± 0.04	0.3 ± 0.01	NS	0.3 ± 0.01	0.4 ± 0.02	NS	0.1–1.1
ALB (g/dl)	2.8 ± 0.11	2.7 ± 0.31	NS	3.1 ± 0.12	3.0 ± 0.10	NS	2.5–5.4

n = 12 mice/group, including 6 males and 6 females; 6 months of age. Mean ± SEM.

ALB, albumin; CHOL, cholesterol; DBILI, direct bilirubin; GLU, glucose; NS, not significant; TBILI, total bilirubin.

mice grew slower than wild-type littermates (supplementary Fig. I-A, B), and the liver/body weight ratio was increased (supplementary Fig. I-C). Histological examination of livers from 12-month-old $Fntb^{\Delta/\Delta}$ mice revealed steatosis, increased collagen staining, apoptosis, and loss of hepatocytes (**Fig. 2**). Steatosis in livers from $Fntb^{\Delta/\Delta}$ mice was confirmed by Oil Red O staining (**Fig. 3A, B**) and electron microscopy (Fig. 3C, D). Liver triglycerides were increased in $Fntb^{\Delta/\Delta}$ mice (Fig. 3E), but there were no significant changes in liver cholesterol levels (Fig. 3F). The serum alanine transaminase (ALT) and aspartate aminotransferase (AST) levels in $Fntb^{\Delta/\Delta}$ mice were markedly elevated, but bilirubin and albumin levels were within normal limits (**Table 1**).

Several abnormalities were readily apparent in hepatocytes isolated from the livers of $Fntb^{\Delta/\Delta}$ mice. First, we observed an increased frequency of nuclei with nuclear blebs (**Fig. 4**). Second, we observed a reduced number of binuclear cells (supplementary Fig. II). Third, many nuclei in $Fntb^{\Delta/\Delta}$ hepatocytes were larger than those in wild-type hepatocytes (supplementary Fig. II). Flow cytometry studies (supplementary Fig. III) revealed a reduced percentage of $Fntb^{\Delta/\Delta}$ cells in the "G_2 phase" (*i.e.,* fewer $Fntb^{\Delta/\Delta}$ hepatocytes had a twice-normal amount of DNA, consistent with the reduced numbers of binuclear hepatocytes).

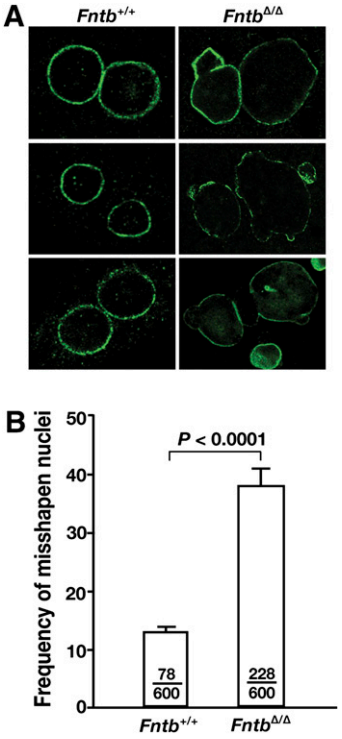

Fig. 4. Misshapen nuclei in $Fntb^{\Delta/\Delta}$ hepatocytes. (A) Immunohistochemical staining of primary hepatocytes from $Fntb^{+/+}$ and $Fntb^{\Delta/\Delta}$ mice with an antibody against lamin A (green). (B) Frequency of misshapen nuclei in $Fntb^{+/+}$ and $Fntb^{\Delta/\Delta}$ hepatocytes. Bars indicate the percentage of cells with misshapen nuclei; the number of cells harboring nuclear blebs and the total number of cells examined are recorded within each bar. Error bars indicate SEM for results with different cell preparations of the same genotype (n = 4/group).

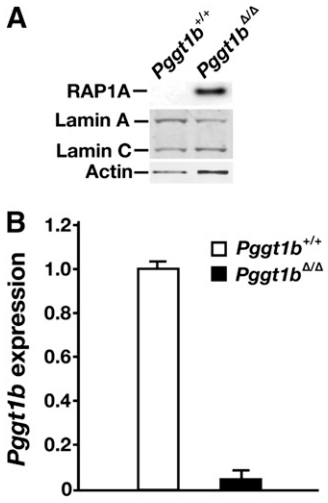

Fig. 5. Inactivating GGTase-I in mouse hepatocytes. (A) Western blot of extracts from primary hepatocyte preparations from $Pggt1b^{+/+}$ and $Pggt1b^{\Delta/\Delta}$ mice with antibodies against nonprenylated RAP1A and lamin A/C. Actin was used as a loading control. (B) Quantitative RT-PCR analysis of *Pggt1b* expression in hepatocytes from $Pggt1b^{+/+}$ and $Pggt1b^{\Delta/\Delta}$ mice (n = 4 mice/group were examined). Data were normalized to β2-microglobulin, and expression levels were compared with levels observed in $Pggt1b^{+/+}$ mice (which was set at 1.0). Error bars indicate SEM.

TABLE 2. Serum chemistry studies in wild-type and *Pggt1b*$^{\Delta/\Delta}$ mice

	Wild-type	*Pggt1b*$^{\Delta/\Delta}$	*P*
ALT (U/L)	39 ± 5	517 ± 91	<0.0001
AST (U/L)	159 ± 36	321 ± 64	<0.0001
ALP (U/L)	51 ± 4	350 ± 34	<0.0001
CHOL (mg/dl)	80 ± 16	121 ± 23	NS
GLU (mg/dl)	296 ± 27	211 ± 21	NS
TRIG (mg/dl)	99 ± 10	87 ± 10	NS
DBILI (mg/dl)	0.1 ± 0.01	32 ± 3	<0.0001
TBILI (mg/dl)	0.2 ± 0.02	35 ± 7	<0.0001

n = 8 mice/group, 8 weeks of age. Mean ± SEM.
CHOL, cholesterol; DBILI, direct bilirubin; GLU, glucose; NS, not significant; TBILI, total bilirubin; TRIG, triglyceride.

Hepatocyte-specific *Pggt1b* knockout mice

A conditional knockout allele for *Pggt1b, Pggt1b*^{fl} (20), and the *AlbCre* transgene were used to produce hepatocyte-specific *Pggt1b* knockout mice (*Pggt1b*$^{fl/fl}$*AlbCre*$^{+}$, designated *Pggt1b*$^{\Delta/\Delta}$ mice). As expected, nonprenylated RAP1A (a protein that is normally geranylgeranylated) could be detected in *Pggt1b*$^{\Delta/\Delta}$ hepatocytes (**Fig. 5A**). *Pggt1b*$^{\Delta/\Delta}$ hepatocytes contained very low levels of *Pggt1b* transcripts (Fig. 5B).

Pggt1b$^{\Delta/\Delta}$ mice survived development and were born at the expected Mendelian ratios. All *Pggt1b*$^{\Delta/\Delta}$ mice had a distended abdomen, beginning at 1 month of age, and were jaundiced. The body weight of *Pggt1b*$^{\Delta/\Delta}$ mice tended to be lower than wild-type mice (supplementary Fig. IV-A, B). The liver and spleen of *Pggt1b*$^{\Delta/\Delta}$ mice were massively enlarged (supplementary Fig. IV-C, D), and serum ALT, AST, and alkaline phosphatase (ALP) levels were markedly elevated, as were total and direct bilirubin levels (**Table 2**). Not surprisingly, the partial thromboplastin and prothrombin times in *Pggt1b*$^{\Delta/\Delta}$ mice were prolonged (**Table 3**). Unlike *Fntb*$^{\Delta/\Delta}$ mice (which appeared healthy at 1 year of age), approximately 50% of *Pggt1b*$^{\Delta/\Delta}$ mice died within 9 weeks of age and all died by 26 weeks of age (supplementary Fig. IV-E).

Hepatocytes from *Pggt1b*$^{\Delta/\Delta}$ mice quickly attached to plastic and ~70% were viable, as judged by trypan blue exclusion, but the cells failed to spread and they manifested an abnormal, rounded shape (supplementary Fig. V-A, B). The nuclei of *Pggt1b*$^{\Delta/\Delta}$ hepatocytes tended to be slightly smaller than those in wild-type hepatocytes (supplementary Fig. V-C, D). The pattern of actin stress filaments in *Pggt1b*$^{\Delta/\Delta}$ hepatocytes was abnormal, as judged by phalloidin staining (supplementary Fig. V-E, F), consistent with the fact that the formation of actin stress fibers depends on geranylgeranylation of RHO GTPases (35).

TABLE 3. Blood coagulation studies in wild-type and *Pggt1b*$^{\Delta/\Delta}$ mice

	Wild-type	*Pggt1b*$^{\Delta/\Delta}$	Normal Range
PTT (second)	8.2 ± 0.21	23.3 ± 0.34	7–19
PT (second)	21.2 ± 1.1	67.6 ± 0.62	18.5–33.4
Fibrinogen (mg/dl)	1.6 ± 0.04	2.1 ± 0.19	1.4–2.1

n = 4 mice/group, 8 weeks of age. Mean ± SEM.
PT, activated prothrombin time; PTT, activated partial thromboplastin time.

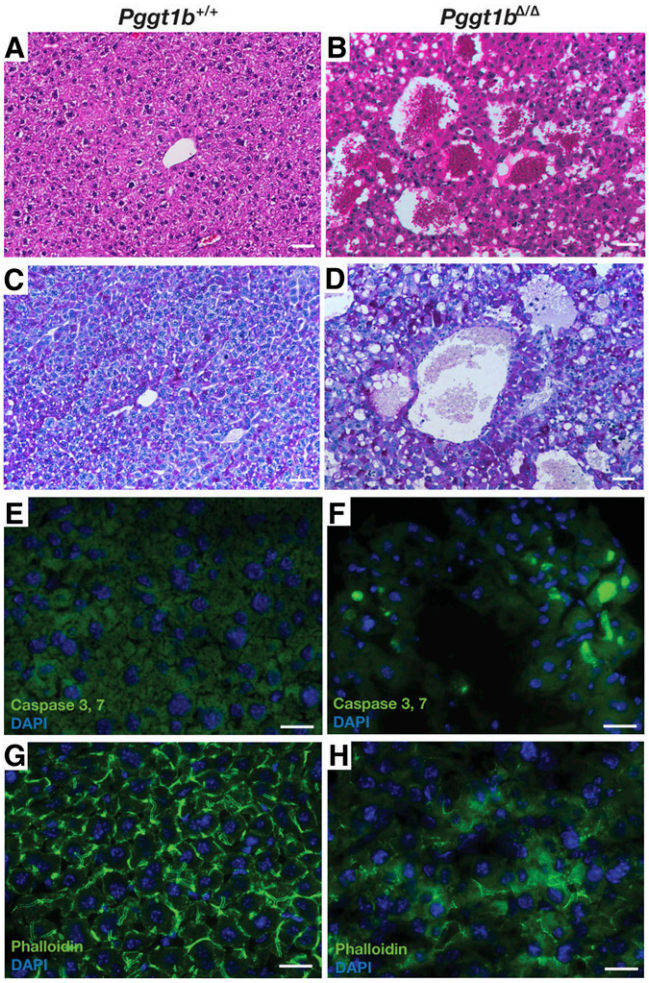

Fig. 6. Severe liver disease in hepatocyte-specific *Pggt1b* knockout mice (*Pggt1b*$^{\Delta/\Delta}$). (A, B) Hematoxylin and eosin–stained liver sections from 4-month-old *Pggt1b*$^{+/+}$ and *Pggt1b*$^{\Delta/\Delta}$ mice, showing disordered hepatic lobules with dilated sinusoids and multiple blood-filled cavities. (C, D) PAS stain revealing increased glycogen (magenta) in the liver of a *Pggt1b*$^{\Delta/\Delta}$ mouse. Images in panels A–D were recorded with a 20× objective. Scale bar, 50 μm. (E, F) In vivo detection of active caspases 3 and 7 (green) in the livers of 4-month-old *Pggt1b*$^{+/+}$ and *Pggt1b*$^{\Delta/\Delta}$ mice (*n* = 3 mice/group were examined). DNA was visualized with DAPI (blue). (G, H) Abnormal organization of actin fibrils in the liver of *Pggt1b*$^{\Delta/\Delta}$ mice, as judged by phalloidin staining (green). DNA was visualized with DAPI (blue). Scale bar for images in panels E–H, 10 μm.

The pattern of tubulin staining within *Pggt1b*$^{\Delta/\Delta}$ cells was also abnormal, likely due to the striking abnormalities in cell shape (supplementary Fig. V-G, H).

The livers of *Pggt1b*$^{\Delta/\Delta}$ mice had necrotic blood-filled cavities, and there appeared to be more glycogen, as judged by a PAS staining (**Fig. 6C, D**). We also observed evidence of apoptosis (caspases 3 and 7 activation) (Fig. 6E, F). In addition, the pattern of actin stress fibers was markedly abnormal (Fig. 6G, H), consistent with findings in isolated hepatocyte preparations (supplementary Fig. V-E, F). Electron microscopy showed markedly dilated bile cannaliculi in livers of *Pggt1b*$^{\Delta/\Delta}$ mice (**Fig. 7**), along with increased amounts of glycogen, smaller and more osmophilic mitochondria, and reduced amounts of rough

endoplasmic reticulum. Some of the dilated bile canaliculi were in direct continuity with the space of Disse (Fig. 7B).

Hepatocyte-specific *Fntb*/*Pggt1b* double-knockout mice

We also bred mice lacking both *Fntb* and *Pggt1b* in hepatocytes ($Fntb^{\Delta/\Delta}Pggt1b^{\Delta/\Delta}$). As expected, hepatocytes from $Fntb^{\Delta/\Delta}Pggt1b^{\Delta/\Delta}$ mice exhibited an accumulation of nonprenylated RAP1A, nonprenylated HDJ-2, and prelamin A (**Fig. 8A, B**). Transcript levels for *Fntb* and *Pggt1b* in $Fntb^{\Delta/\Delta}Pggt1b^{\Delta/\Delta}$ hepatocytes were very low (Fig. 8C, D).

Like $Pggt1b^{\Delta/\Delta}$ mice, the $Fntb^{\Delta/\Delta}Pggt1b^{\Delta/\Delta}$ mice had markedly enlarged abdomens, and their body weights were lower than in wild-type mice (supplementary Fig. VI). The lifespan of $Fntb^{\Delta/\Delta}Pggt1b^{\Delta/\Delta}$ mice was slightly shorter than in $Pggt1b^{\Delta/\Delta}$ mice (supplementary Fig. IV-E).

Hepatocytes from $Fntb^{\Delta/\Delta}Pggt1b^{\Delta/\Delta}$ mice exhibited the same rounded shape as $Pggt1b^{\Delta/\Delta}$ hepatocytes (supplementary Fig. VII-A, B). Also, compared with wild-type hepatocytes, there were fewer numbers of binuclear hepatocytes and increased numbers of cells with enlarged nuclei (supplementary Fig. VII-C–E). Liver histology in $Fntb^{\Delta/\Delta}Pggt1b^{\Delta/\Delta}$ mice was markedly abnormal, with areas of necrosis and increased collagen staining (**Fig. 9A–D**). The reticulin stain revealed multiple areas of hepatocyte loss (Fig. 9E, F). The serum ALT, AST, and ALP levels in $Fntb^{\Delta/\Delta}Pggt1b^{\Delta/\Delta}$ mice (**Table 4**) were higher than we observed in $Fntb^{\Delta/\Delta}$ or $Pggt1b^{\Delta/\Delta}$ mice (Tables 1 and 2), but we did not find extremely high levels of bilirubin in $Fntb^{\Delta/\Delta}Pggt1b^{\Delta/\Delta}$ mice.

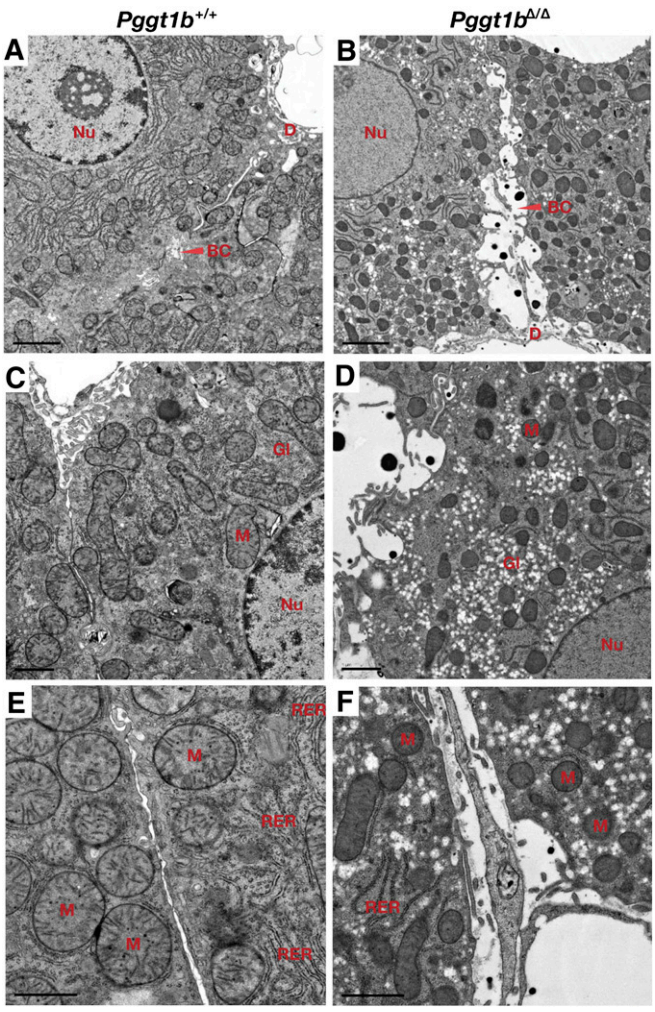

Fig. 7. Electron micrographs of livers from $Pggt1b^{+/+}$ and $Pggt1b^{\Delta/\Delta}$ mice (A–F). $Pggt1b^{\Delta/\Delta}$ livers exhibit dilated bile canaliculi (B), increased amounts of glycogen (D), smaller and darker-staining mitochondria (D, F), and reduced amounts of rough endoplasmic reticulum (F). BC, bile canaliculus; D, space of Disse; Gl, glycogen; M, mitochondria; Nu, nucleus; RER, rough endoplasmic reticulum. Magnification in panels A–B, ×14,000; scale bar, 2.0 μm. Magnification in panels C–D, ×23400; scale bar, 1.0 μm. Magnification in panels E–F, ×37,400; scale bar, 1.0 μm.

DISCUSSION

The importance of protein isoprenylation for targeting *CaaX* proteins to membrane surfaces has been well documented in cell culture studies (2), but the physiologic relevance and importance of these posttranslational modifications for the vitality and viability of mammalian tissues has remained unclear. In the current study, we show that inactivation of either *Fntb* or *Pggt1b* in hepatocytes causes severe hepatocellular disease, with elevated plasma transaminases and histological evidence of hepatocyte damage and hepatocyte loss. But while hepatocellular disease was a shared feature of the two knockout models, several phenotypes were distinct. Most impressively, the *Pggt1b* knockout led to markedly elevated bilirubin and alkaline phosphatase levels, along with severe hepatosplenomegaly. The *Fntb* knockout also had unique features—hepatic steatosis, reduced numbers of binuclear hepatocytes, and more misshapen cell nuclei. These studies show that FTase-deficient cells are *not* free of pathology and that FTase is *not* dispensable in adult mice, as was suggested earlier (12), and they further demonstrated that GGTase-I deficiency is devastating for liver function. The knockout of both *CaaX* prenyltransferases resulted in more severe hepatocellular disease, as judged by reduced survival and exaggerated increases in serum transaminases. The fact that the liver in $Fntb^{\Delta/\Delta}Pggt1b^{\Delta/\Delta}$ mice develops and functions (albeit at a minimal level) in the absence of both FTase and GGTase-I was remarkable, given that the loss of both prenyltransferases in yeast is lethal (13, 36).

From a technical standpoint, the knockouts of *Fntb* and *Pggt1b* in the liver worked well. The β-subunit of the FTase was undetectable in livers of $Fntb^{\Delta/\Delta}$ mice, and most of the HDJ-2 in $Fntb^{\Delta/\Delta}$ hepatocytes was nonprenylated. The levels of *Fntb* transcripts in livers of $Fntb^{\Delta/\Delta}$ mice were extremely low, as were *Pggt1b* transcripts levels in livers of $Pggt1b^{\Delta/\Delta}$ mice. However, the transcripts in the knockout models were not completely eliminated, and that was not surprising. First, the albumin–*Cre* transgene inactivates floxed genes within hepatocytes, but not other liver cell types. Also, the *Fntb* and *Pggt1b* knockouts caused apoptosis, which likely caused an influx of inflammatory cells with normal levels of *Fntb* and *Pggt1b* expression.

In an earlier study, Mijimolle et al. (12) concluded that a generalized deficiency in FTase caused few or no histological abnormalities, but in the current study, we found severe hepatocellular disease. What explains this

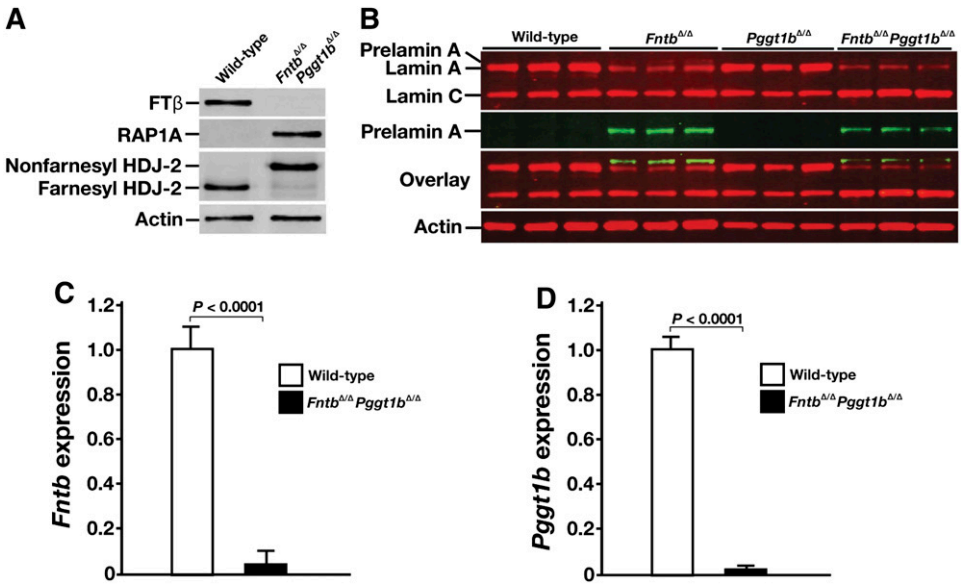

Fig. 8. Inactivating both FTase and GGTase-I in mouse hepatocytes. (A) Western blots of hepatocytes from wild-type and $Fntb^{\Delta/\Delta}Pggt1b^{\Delta/\Delta}$ mice with antibodies against the β-subunit of FTase (FTβ), nonprenylated RAP1A, and HDJ-2. (B) Western blots of hepatocyte extracts from wild-type, $Fntb^{\Delta/\Delta}$, $Pggt1b^{\Delta/\Delta}$, and $Fntb^{\Delta/\Delta}Pggt1b^{\Delta/\Delta}$ mice with antibodies against lamin A/C and prelamin A ($n = 3$ hepatocyte preparations/group). Actin was used as loading control. (C, D) Quantitative RT-PCR analysis of *Fntb* (C) and *Pggt1b* (D) expression in hepatocytes from wild-type and $Fntb^{\Delta/\Delta}Pggt1b^{\Delta/\Delta}$ mice ($n = 4$ hepatocyte preparations/group). Data were normalized to β2-microglobulin, and gene-expression levels were compared with those of wild-type mice (set at 1.0). Error bars indicate SEM.

discrepancy? We suspect that Mijimolle and coworkers were simply unsuccessful in inactivating FTase. Their mutant allele yielded a short in-frame deletion within the *Fntb* transcript—not the frameshift that they had hoped for (37); hence, it seems possible that their mutant allele may not have inactivated enzyme function. In support of this explanation, they found that a large percentage of the HDJ-2 in *cloned* "knockout" fibroblasts was prenylated. With our mutant allele, the recombination event eliminated the promoter and exon 1, and the vast majority of the HDJ-2 in hepatocytes was nonprenylated. Also, in their studies, Mijimolle and coworkers relied on a ubiquitously expressed inducible *Cre* transgene, and it seems possible that their recombination rates were far lower than they expected—and far lower than we obtained with the albumin–*Cre* transgene.

In the current studies, the knockout of *Fntb* in the liver led to an accumulation of prelamin A, in agreement with cell culture studies where protein prenylation was inhibited with statins (38), FTIs (31, 39–41), or bisphophonates (30). We also observed reduced levels of mature lamin A in the setting of the *Fntb* knockout—a finding that did not surprise us. In earlier studies (30), we found a striking decrease in mature lamin A levels in mouse fibroblasts that had been treated with an FTI. We did not observe an accumulation of prelamin A in $Pggt1b^{\Delta/\Delta}$ hepatocytes, consistent with the fact that prelamin A is normally farnesylated. The prelamin A Western blot on independent preparations of hepatocytes from $Fntb^{\Delta/\Delta}Pggt1b^{\Delta/\Delta}$ mice were interesting, particularly in light of the suggestion by Varela et al. (42) that prelamin A is geranylgeranylated by GGTase-I in the setting of FTase inhibition. In support of their idea, they reported that a FTI/GGTI combination led to more prelamin A accumulation than an FTI alone, but the specificity of their drugs was not well documented. In our studies, the levels of prelamin A accumulation were no greater in $Fntb^{\Delta/\Delta}Pggt1b^{\Delta/\Delta}$ hepatocytes than in $Fntb^{\Delta/\Delta}$ hepatocytes, providing little support for the idea that prelamin A is alternately prenylated. However, caution is warranted in the interpretation of these experiments because we detected mature lamin A, as well as small amounts of prenylated HDJ-2, in the $Fntb^{\Delta/\Delta}Pggt1b^{\Delta/\Delta}$ hepatocytes, indicating that the hepatocyte preparations may have been contaminated with other cell types.

Previous studies have shown that geranylgeranylation of RHO GTPases is critical for the formation of actin stress fibers within cells (35). Our studies support that finding. Cultured GGTase-I–deficient hepatocytes exhibited a marked depletion of actin stress fibers, as judged by phalloidin staining, and they had a markedly abnormal, rounded shape. Abnormal organization of actin stress fibers was also evident in the livers of $Pggt1b^{\Delta/\Delta}$ mice. We suspect that the defects in the hepatocyte cytoskeleton may have contributed to the hyperbilirubinemia in $Pggt1b^{\Delta/\Delta}$ mice. In $Pggt1b^{\Delta/\Delta}$ livers, adjacent hepatocytes were often separated, and the cannaliculi between cells were frequently enlarged. Occasionally, bile cannaliculi were in direct continuity with the space of Disse, providing a likely explanation for the elevated levels of bilirubin in the plasma.

In summary, we found that deficiencies in either FTase or GGTase-I lead to severe hepatocellular disease. Our

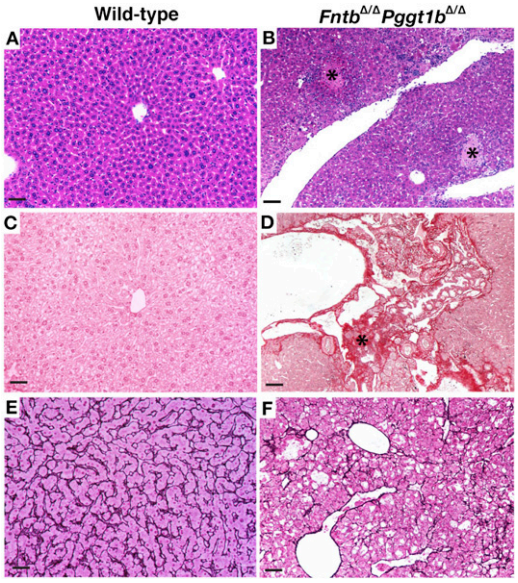

Fig. 9. Inactivation of both *Fntb* and *Pggt1b* in liver causes severe hepatocellular disease. (A, B) Hematoxylin and eosin–stained sections of liver from 3-month-old wild-type and $Fntb^{\Delta/\Delta}Pggt1b^{\Delta/\Delta}$ mice, revealing disordered hepatic lobules and areas of necrosis (black asterisks) in $Fntb^{\Delta/\Delta}Pggt1b^{\Delta/\Delta}$ mice. (C, D) Sirius Red–stained liver sections, revealing increased amounts of collagen in the liver of $Fntb^{\Delta/\Delta}Pggt1b^{\Delta/\Delta}$ mouse. Black asterisks in panels B and D indicate areas of necrosis. (E, F) Liver sections from 4-month-old wild-type and $Fntb^{\Delta/\Delta}Pggt1b^{\Delta/\Delta}$ mice stained for reticulin, revealing disorganized liver architecture, lipid globules, and areas of hepatocyte loss. Images were recorded with a 20× objective. Scale bars, 50 μm.

studies lay to rest the earlier notion that FTase is dispensable in adult tissues. Our studies do not speak to the potential utility of FTIs and GGTIs as anticancer agents, either alone or in combination with each other or other agents. However, our findings imply that pharmacological inhibition of FTase and GGTase-I, if it were sustained and complete, could cause significant injury to the liver and other tissues.

The authors thank Drs. Pinchas Cohen (UCLA) for the albumin–*Cre* transgenic mice, Larry Castellani (UCLA) for some of the hepatocyte preparations, Ingrid Schmid (UCLA) for flow cytometry analysis, and Ms. Jinny Wong (UCSF) for electron microscopy.

TABLE 4. Serum chemistry studies in wild-type and $Fntb^{\Delta/\Delta}$ $Pggt1b^{\Delta/\Delta}$ mice

	Wild-type	$Fntb^{\Delta/\Delta}$ $Pggt1b^{\Delta/\Delta}$	*P*
ALT (U/L)	39 ± 5	1201 ± 48	<0.0001
AST (U/L)	159 ± 36	1487 ± 72	<0.0001
ALP (U/L)	51 ± 4	1501 ± 47	<0.0001
CHOL (mg/dl)	80 ± 16	69 ± 8	NS
GLU (mg/dl)	296 ± 27	87 ± 11.3	NS
TRIG (mg/dl)	99 ± 10	52 ± 7.6	NS
DBILI (mg/dl)	0.1 ± 0.02	9.45 ± 3.62	<0.0001
TBILI (mg/dl)	0.2 ± 0.01	13.7 ± 3.41	<0.0001

CHOL, cholesterol; GLU, glucose; DBILI, direct bilirubin; NS, not significant; TBILI, total bilirubin; TRIG, triglyceride.

n = 8 mice/group, 6–8 weeks of age. Mean ± SEM.

REFERENCES

1. Casey, P. J., and M. C. Seabra. 1996. Protein prenyltransferases. *J. Biol. Chem.* **271:** 5289–5292.
2. Zhang, F. L., and P. J. Casey. 1996. Protein prenylation: molecular mechanisms and functional consequences. *Annu. Rev. Biochem.* **65:** 241–269.
3. Casey, P. J., P. A. Solski, C. J. Der, and J. E. Buss. 1989. p21ras is modified by a farnesyl isoprenoid. *Proc. Natl. Acad. Sci. USA.* **86:** 8323–8327.
4. Hancock, J. F., A. I. Magee, J. E. Childs, and C. J. Marshall. 1989. All *ras* proteins are polyisoprenylated but only some are palmitoylated. *Cell.* **57:** 1167–1177.
5. Cox, A. D., M. M. Hisaka, J. E. Buss, and C. J. Der. 1992. Specific isoprenoid modification is required for function of normal, but not oncogenic, Ras protein. *Mol. Cell. Biol.* **12:** 2606–2615.
6. Lerner, E. C., A. D. Hamilton, and S. M. Sebti. 1997. Inhibition of Ras prenylation: a signaling target for novel anti-cancer drug design. *Anticancer Drug Des.* **12:** 229–238.
7. Gibbs, J. B., A. Oliff, and N. E. Kohl. 1994. Farnesyltransferase inhibitors: Ras research yields a potential cancer therapeutic. *Cell.* **77:** 175–178.
8. Tamanoi, F. 1993. Inhibitors of Ras farnesyltransferases. *Trends Biochem. Sci.* **18:** 349–353.
9. James, G. L., J. L. Goldstein, M. S. Brown, T. E. Rawson, T. C. Somers, R. S. McDowell, C. W. Crowley, B. K. Lucas, A. D. Levinson, and J. C. Marsters, Jr. 1993. Benzodiazepine peptidomimetics: potent inhibitors of Ras farnesylation in animal cells. *Science.* **260:** 1937–1942.
10. Sebti, S. M., and A. D. Hamilton. 2000. Farnesyltransferase and geranylgeranyltransferase I inhibitors and cancer therapy: lessons from mechanism and bench-to-bedside translational studies. *Oncogene.* **19:** 6584–6593.
11. Lobell, R. B., C. A. Omer, M. T. Abrams, H. G. Bhimnathwala, M. J. Brucker, C. A. Buser, J. P. Davide, S. J. deSolms, C. J. Dinsmore, M. S. Ellis-Hutchings, et al. 2001. Evaluation of farnesyl:protein transferase and geranylgeranyl:protein transferase inhibitor combinations in preclinical models. *Cancer Res.* **61:** 8758–8768.
12. Mijimolle, N., J. Velasco, P. Dubus, C. Guerra, C. A. Weinbaum, P. J. Casey, V. Campuzano, and M. Barbacid. 2005. Protein farnesyltransferase in embryogenesis, adult homeostasis, and tumor development. *Cancer Cell.* **7:** 313–324.
13. He, B., P. Chen, S-Y. Chen, K. L. Vancura, S. Michaelis, and S. Powers. 1991. *RAM2*, an essential gene of yeast, and *RAM1* encode the two polypeptide components of the farnesyltransferase that prenylates a-factor and Ras proteins. *Proc. Natl. Acad. Sci. USA.* **88:** 11373–11377.
14. Vallim, M. A., L. Fernandes, and J. Alspaugh. 2004. The RAM1 gene encoding a protein-farnesyltransferase β-subunit homologue is essential in Cryptococcus neoformans. *Microbiology.* **150:** 1925–1935.
15. Hanrahan, E. O., M. Kies, B. Glisson, F. Khuri, L. Feng, H. Tran, L. Ginsberg, M. Truong, W. Hong, and E. Kim. 2009. A phase II study of Lonafarnib (SCH66336) in patients with chemorefractory, advanced squamous cell carcinoma of the head and neck. *Am. J. Clin. Oncol.* **32:** 274–279.
16. Santucci, R., P. Mackley, S. Sebti, and M. Alsina. 2003. Farnesyltransferase inhibitors and their role in the treatment of multiple myeloma. *Cancer Control.* 10**:** 384–387.
17. Lee, R., S. Y. Chang, H. Trinh, Y. Tu, A. C. White, B. S. Davies, M. O. Bergo, L. G. Fong, W. E. Lowry, and S. G. Young. 2010. Genetic studies on the functional relevance of the protein prenyltransferases in skin keratinocytes. *Hum. Mol. Genet.* **19:** 1603–1617.
18. Kazi, A., A. Carie, M. Blaskovich, C. Bucher, V. Thai, S. Moulder, H. Peng, D. Carrico, E. Pusateri, W. Pledger, et al. 2009. Blockade of protein geranylgeranylation inhibits cdk2-dependent p27Kip1 phosphorylation on thr187 and accumulates p27Kip1 in the nucleus: implications for breast cancer therapy. *Mol. Cell. Biol.* **29:** 2254–2263.
19. Lu, J., L. Chan, H. Fiji, R. Dahl, O. Kwon, and F. Tamanoi. 2009. In vivo antitumor effect of a novel inhibitor of protein geranylgeranyltransferase I. *Mol. Cancer Ther.* **8:** 1218–1226.
20. Sjogren, A. K., K. M. Andersson, M. Liu, B. A. Cutts, C. Karlsson, A. M. Wahlstrom, M. Dalin, C. Weinbaum, P. J. Casey, A. Tarkowski, et al. 2007. GGTase-I deficiency reduces tumor formation and improves survival in mice with K-RAS-induced lung cancer. *J. Clin. Invest.* **117:** 1294–1304.

21. Liu, M., A. Sjogren, C. Karlsson, M. Lbrahim, K. Andersson, F. Olofsson, A. Wahistrom, M. Dalin, H. Yu, Z. Chen, et al. 2010. Targeting the protein prenyltransferases efficiently reduces tumor development in mice with K-RAS-induced lung cancer. *Proc. Natl. Acad. Sci. USA.* **107:** 6471–6476.
22. Khan, O. M., M. X. Ibrahim, I. Jonsson, C. Karlsson, M. Liu, A. Sjogren, F. Olofsson, M. Brisslert, S. Andersson, C. Ohlsson, et al. 2011. Geranylgeranyltransferase type I (GGTase-I) deficiency hyperactivates macrophages and induces erosive arthritis in mice. *J. Clin. Invest.* **121:** 628–639.
23. Weisend, C. M., J. Kundert, E. Suvorova, J. Prigge, and E. Schmidt. 2009. Cre activity in fetal albCre mouse hepatocytes: utility for developmental studies. *Genesis.* **47:** 789–792.
24. Anzo, M., L. Cobb, D. Hwang, H. Mehta, J. Said, S. Yakar, D. LeRoith, and P. Cohen. 2008. Targeted deletion of hepatic Igf1 in TRAMP mice leads to dramatic alterations in the circulating insulin-like growth factor axis but does not reduce tumor progression. *Cancer Res.* **68:** 3342–3349.
25. Seglen, P. O. 1976. Preparation of isolated rat liver cells. *Methods Cell Biol.* **13:** 29–83.
26. Klaunig, J. E., P. Goldblatt, D. Hinton, M. Lipsky, J. Chacko, and B. Trump. 1981. Mouse liver cell culture. I. Hepatocyte isolation. *In Vitro.* **17:** 913–925.
27. Livak, K. J., and T. Schmittgen. 2001. Analysis of relative gene expression data using real-time quantitative PCR and the 2(-Delta Delta C(T)) method. *Methods.* **25:** 402–408.
28. Fong, L. G., J. K. Ng, M. Meta, N. Cote, S. H. Yang, C. L. Stewart, T. Sullivan, A. Burghardt, S. Majumdar, K. Reue, et al. 2004. Heterozygosity for Lmna deficiency eliminates the progeria-like phenotypes in Zmpste24-deficient mice. *Proc. Natl. Acad. Sci. USA.* **101:** 18111–18116.
29. Fong, L. G., J. K. Ng, J. Lammerding, T. A. Vickers, M. Meta, N. Cote, B. Gavino, X. Qiao, S. Y. Chang, S. R. Young, et al. 2006. Prelamin A and lamin A appear to be dispensable in the nuclear lamina. *J. Clin. Invest.* **116:** 743–752.
30. Toth, J. I., S. H. Yang, X. Qiao, A. P. Beigneux, M. H. Gelb, C. L. Moulson, J. H. Miner, S. G. Young, and L. G. Fong. 2005. Blocking protein farnesyltransferase improves nuclear shape in fibroblasts from humans with progeroid syndromes. *Proc. Natl. Acad. Sci. USA.* **102:** 12873–12878.
31. Yang, S. H., M. O. Bergo, J. I. Toth, X. Qiao, Y. Hu, S. Sandoval, M. Meta, P. Bendale, M. H. Gelb, S. G. Young, et al. 2005. Blocking protein farnesyltransferase improves nuclear blebbing in mouse fibroblasts with a targeted Hutchinson-Gilford progeria syndrome mutation. *Proc. Natl. Acad. Sci. USA.* **102:** 10291–10296.
32. Yang, S. H., D. Andres, H. Spielmann, S. Young, and L. Fong. 2008. Progerin elicits disease whether or not it is farnesylated. *J. Clin. Invest.* **118:** 3291–3300.
33. Steinert, P., R. Zackroff, M. Aynardi-Whitman, and R. D. Goldman. 1982. Isolation and characterization of intermediate filaments. *Methods Cell Biol.* **24:** 399–419.
34. Folch, J., M. Lees, and G. H. S. Stanley. 1957. A simple method for the isolation and purification of total lipides from animal tissues. *J. Biol. Chem.* **226:** 497–509.
35. Hall, A. 1998. Rho GTPases and the actin cytoskeleton. *Science.* **279:** 509–514.
36. Powers, S., S. Michaelis, D. Broek, S. S. Anna-A., J. Field, I. Herskowitz, and M. Wigler. 1986. *RAM*, a gene of yeast required for a functional modification of *RAS* proteins and for production of mating pheromone a-factor. *Cell.* **47:** 413–422.
37. Yang, S. H., M. O. Bergo, E. Farber, X. Qiao, L. G. Fong, and S. G. Young. 2009. Caution! Analyze transcripts from conditional knockout alleles. *Transgenic Res.* **18:** 483–489.
38. Sinensky, M., L. A. Beck, S. Leonard, and R. Evans. 1990. Differential inhibitory effects of lovastatin on protein isoprenylation and sterol synthesis. *J. Biol. Chem.* **265:** 19937–19941.
39. Yang, S. H., M. Meta, X. Qiao, D. Frost, J. Bauch, C. Coffinier, S. Majumdar, M. O. Bergo, S. G. Young, and L. G. Fong. 2006. Treatment with a protein farnesyltransferase inhibitor improves disease phenotypes in mice with a targeted Hutchinson-Gilford progeria syndrome mutation. *J. Clin. Invest.* **116:** 2115–2121.
40. Fong, L. G., D. Frost, M. Meta, X. Qiao, S. Yang, C. Coffinier, and S. Young. 2006. A protein farnesyltransferase inhibitor ameliorates disease in a mouse model of progeria. *Science.* **311:** 1621–1623.
41. Young, S. G., M. Meta, S. H. Yang, and L. G. Fong. 2006. Prelamin A farnesylation and progeroid syndromes. *J. Biol. Chem.* **281:** 39741–39745.
42. Varela, I., S. Pereira, A. P. Ugalde, C. L. Navarro, M. F. Suarez, P. Cau, J. Cadinanos, F. G. Osorio, N. Foray, J. Cobo, et al. 2008. Combined treatment with statins and aminobisphosphonates extends longevity in a mouse model of human premature aging. *Nat. Med.* **14:** 767–772.